Journal of Bone and Mineral Metabolism (2019) 37:399–410
https://doi.org/10.1007/s00774-018-0939-7

ORIGINAL ARTICLE

Metformin protects bone mass in ultra-high-molecular-weight polyethylene particle-induced osteolysis by regulating osteocyte secretion

Zhao Yan[1] · Shu Zhu[1] · Xiaoxi Tian[2] · Zichen Ye[3] · Dongsheng Zhai[3] · Zheng Zhu[4] · Di Wei[4] · Qingsheng Zhu[1] · Zifan Lu[3] · Xiaorui Cao[1]

Received: 9 November 2017 / Accepted: 17 June 2018 / Published online: 21 July 2018

Abstract

Metformin, an anti-hyperglycemic agent used for type 2 diabetes, has recently been found to have more effects apart from glucose regulation. We found that, in ultra-high-molecular-weight polyethylene particle-induced osteolysis mouse models, metformin had bone protect property and reduced the negative regulator of bone formation sclerostin (SOST) and Dickkopf-related protein 1 (DKK1), and increased osteoprotegerin (OPG) secretion and the ratio of OPG/Receptor Activator for Nuclear Factor-κB Ligand (RANKL). In vitro, we established a 3D co-culture system in which metformin affects osteoblasts and osteoclasts through mature osteocytes secretion. Metformin (50 μM) significantly decreased SOST and DKK1 mRNA expression, stimulating alkaline phosphatase activity and proliferation of osteoblast, and increased OPG secretion and the ratio of OPG/RANKL, inhibiting osteoclastogenesis. Moreover, the effect on OPG was reversed by adenosine 5′-monophosphate-activated protein kinase inhibitor, Compound C. Our finding suggests that metformin induces differentiation and mineralization of osteoblasts, while inhibits osteoclastogenesis via mature osteocytes secretion. Therefore, the drug might be beneficial for not only diabetes but also in other bone disorders by acting on mature osteocytes.

Keywords Metformin · Osteocyte · Sclerostin · DKK1 · OPG

Introduction

Long-term outcomes of total joint arthroplasty (TJA) have been confined by periprosthetic osteolysis caused mainly by ultra-high-molecular-weight polyethylene (UHMWPE) wear debris. Aseptic loosening was a major cause of TJA failure in the late period and overall in both periods [1]. Bone disorders such as osteoporosis are caused by dysfunction of balanced osteocyte regulation, and treatments for these diseases like anti-inflammation drugs and bisphosphonates have unavoidable complications such as gastrointestinal complications and osteonecrosis [2]. Therefore, it is of high value to find a new drug for bone disorders with minimized side effects.

Osteocyte is the dominating cell in human bone tissue, accounting for more than 90% of total cell number, about 20 times of osteoblasts number. It comes from osteoblast, but survives much longer. Recently, osteocyte's endocrine function has been discovered [3, 4], indicating its significant role in bone function and metabolism. Given the proportion

Zhao Yan, Shu Zhu, and Xiaoxi Tian have contributed equally to this work.

✉ Zifan Lu
luzfliuq@fmmu.edu.cn

✉ Xiaorui Cao
caoxr@fmmu.edu.cn

[1] Department of Orthopaedics, Xijing Hospital, Fourth Military Medical University, Xi'an 710032, People's Republic of China

[2] Emergency Department of Tangdu Hospital, Fourth Military Medical University, Xi'an 710032, People's Republic of China

[3] State Key Laboratory of Cancer Biology, Department of Pharmacogenomics, Fourth Military Medical University, Xi'an 710032, People's Republic of China

[4] Department of Urinary Surgery, Xijing Hospital, Fourth Military Medical University, Xi'an 710032, People's Republic of China

and longevity of mature osteocyte, regulating its secretion may bring unexpected results in treatment of bone disorders.

Metformin is an anti-hyperglycemia drug used for type 2 diabetes mellitus. Its role as an adenosine 50-monophosphate (AMP)-activated protein kinase (AMPK) activator is the key of the metabolism regulating effects. Its possible role in bone metabolism is still controversial. Evidence shows that metformin administration does not help to alleviate postmenopausal diabetic osteoporosis and facilitate fracture healing [5, 6]. However, there is also evidence showing that metformin may stimulate osteoblast differentiation through the transactivation of Runx2 via AMPK/USF-1/SHP regulatory cascade [7] and reduce bone loss in mouse [8]. Moreover, metformin induces osteoblastic differentiation of human-induced pluripotent stem cell-derived mesenchymal stem cells via activation of the LKB1/AMP-activated protein kinase (AMPK) signaling pathway [9].

In this study, we explored metformin's potential effect on ultra-high-molecular-weight polyethylene (UHWMPE) particle-induced osteolysis mouse model, and we also examined the possible mechanism of the effect in vitro in the 3D culture system. Administration of metformin could help to reduce osteolysis, promote bone formation, and inhibit osteoclastogenesis by regulating sclerostin (SOST), DKK1, OPG, and RANKL by mature osteocyte. Blocking of AMPK signal pathway reversed the elevation of OPG induced by metformin. Thus, we hypothesize that metformin might affect mature osteocytes in an endocrinic manner and protect bone mass in bone metabolic abnormalities.

Materials and methods

Preparation of UHMWPE particles and biphasic calcium phosphate (BCP) particles

The average diameter of the UHMWPE particles (provided by Prof. Liu Hongtao of China University of Mining and Technology) was < 1 μm (ranging from 0.05 to 0.9 μm). Notably, this particle diameter is within the range considered biologically active and differs from the diameter of particles isolated from the periprosthetic membranes. All particles were rinsed to remove the endotoxins using ethanol before desiccation in drying oven, and correspondingly, tests for endotoxins using the Limulus assay (Sigma-Aldrich, St. Louis, MO, USA) were negative. Before use in cell culture, the particles were disinfected under γ-irradiation in air (2.5 MR) and kept at 4 °C. The particles were exposed to UV light for 1 h immediately before use as previously described [10]. BCP microbeads were provided by Prof. Liu Hongtao of China University of Mining and Technology, composed of 68% of hydroxyapatite and 32% of β-tricalcium phosphate as described previously [11]. The microbeads size ranges from 20 to 25 μm. All particles are sterilized by heating to 180 °C for 2 h and are coated with collagen type-I (Sigma-Aldrich, MO, USA) using a collagen/acetic acid solution (0.15 mg/mL), stored in 4 °C for further use.

BCP-coated coverslips

Glass coverslips were coated with BCP microbeads according to the procedure reported previously [11]. In brief, BCP microbeads were placed in dimethyl sulfoxide (DMSO; 1 mg particles in 0.5 mL DMSO) in a sterile quartz pestle and mortar. Subsequently, the materials were suspended in 14.5 mL of collagen type-I monomer (0.01%) solution (C-8919; Sigma-Aldrich) and stored at 4 °C. The final particle concentration was set at 10^7 particle/mL. The microscope coverslips with dimensions of 22 × 22 mm (Dingjie Biological Technology Co., Ltd., Shanghai, China) were disinfected for 2 h at 200 °C. Collagen-suspended particles (10^5 particles/10 μL) were distributed onto the coverslip uniformly. In control samples, coverslips were only coated with collagen and BCP particles without cells. The coverslips were placed into 6-well tissue culture plates before irradiation with ultraviolet light overnight in a sterile tissue culture hood. The plates were placed in PE packages and covered with aluminum foil in 4 °C. Another 1 h exposure in ultraviolet light was performed immediately before usage of the coverslips.

Cell culture and cell viability

Cells (primary mouse osteocytes, osteoblasts, and BMMs) were cultured in Dulbecco's Modified Eagle Medium (DMEM) supplemented with 10% fetal bovine serum (FBS; Gibco) and penicillin (100 U/mL). BMMs were obtained from mouse femurs as described previously [12]. Primary osteoblasts were obtained from the calvaria from neonatal mouse pups (age 3–4 days) according to protocol by Takahashi [13].

Mature osteocyte culture system was based on the previous work by Boukhechba [14]. Primary mouse osteoblasts were obtained according to protocols and were seeded on BCP microbead-coated 24-well culture plate in differentiation medium (DMEM, 10% FCS, 50 μg/mL ascorbic acid, and 10 mM β-glycerophosphate) for 14 days and medium was changed every day. The differentiation process was visualized by mRNA expression of osteocyte markers and by Alizarin red S staining for calcium deposition. After differentiated mature osteocytes were confirmed, 200 μL of primary osteoblasts or BMMs suspension at a concentration of 10^7 cells/mL was added to each insert to form the 3D culture system (Fig. 3a). The cells were placed at 37.8 °C and 5% CO_2. Metformin solution was added to each well but not insert at a concentration of 10, 25, and 50 μM with or without 40 μM Compound C. Osteoclast differentiation

medium containing M-CSF (10 ng/mL) and mouse RANKL (10 ng/mL) was added into BMMs inserts to see the effects on osteoclastogenesis for 1 week. Twenty-four hours after metformin administration, cells and culture supernate in each well were collected for further use.

Cell proliferation of osteoblast was assessed using the cell counting kit (CCK-8) assay (Dojindo Molecular Technologies Inc., Rockville, MD, USA) according to the instructions. Osteoblast was seeded in 96-well plates with 100 µL/well. Then, medium was replaced with mature osteocyte supernatant treated with various concentrations of metformin for 24 h. After incubation, 10 µL of CCK-8 solution was added to each well and incubated for 2 h at 37 °C. As an indicator, optical density was examined at a wavelength of 450 nm.

RNA extraction and real-time PCR

According to the manufacturer's suggestions, RNAs from calvaria specimens (soft tissue shaved from bone) or cells were purified with Trizol reagent (Invitrogen, Carlsbad CA, USA). The synthesis of cDNA was operated using murine leukemia virus (M-MLV) reverse transcriptase and performed using random primers (Invitrogen, Carlsbad, CA, USA). An ABI7500 system (Applied Biosystems, Foster City, CA, USA) was used to perform the real-time PCR (RT-PCR). Each reaction volume contained the 5′ primer (0.5 µM), 3′ primer (0.5 µM), SYBR Green I (10 µL, Takara, Dalian, China), sample (2 µL), and H_2O to the final volume of 20 µL. For 45 cycles, samples were amplified with a denaturation step at 95 °C for 5 s, before the annealing and extension steps at 60 °C for 34 s. The amount of double-stranded DNA was determined by measuring SYBR green fluorescence. A melting curve was generated after each run, to distinguish between the specific and nonspecific cDNA products. The relative mRNA levels of target genes were normalized to the β-actin levels and compared with those in control samples. The primers used are listed in Table 1:

ELISA assay of cytokines

Calvaria were harvested and soft tissues were completely removed before grinded in liquid nitrogen. PBS was added to dissolve protein. Levels of SOST, DKK1, OPG, and RANKL in calvaria and cell supernates were determined using Mouse/Rat Quantikine ELISA Kit (R&D Systems, Minneapolis, MN, USA). Supernate levels of inflammatory cytokines TNF-α, IL-6, and IL-10 were measured using Mouse/Rat Quantikine ELISA Kit (R&D Systems, Minneapolis, MN, USA) after centrifugalization. All assays were performed according to the manufacturer's instructions.

Table 1 Primers of genes used in Real-Time PCR

	Primers
SOST	F, 5′-AGGAATGATGCCACAGAGGT-3′ R, 5′-TTTGGCGTCATAGGGATGGT-3′
DKK1	F, 5′-CAAGCACAAACGGAAAGGCT-3′ R, 5′-TGCTGGCTTGATGGTGATCT-3′
OPG	F, 5′-CACACGAACTGCAGCACATT-3′ R, 5′-ATTCCACACTTTTGCGTGGC-3′
RANKL	F, 5′-TACTCGTAGCTAAGGGGGCA-3′ R, 5′-CACCTGGTGACCAACATCCT-3′
ALPL	F, 5′-CAGGCCGCCTTCATAAGCA-3′ R, 5′-AATTGACGTTCCGATCCTGC-3′
DMP1	F, 5′-CGCTGAGGTTTTGACCTTGT-3′ R, 5′-TGATGACTCACTGTTCGTGGG-3′
FGF23	F, 5′-GGCACTGCTAGAGCCTATCC-3′ R, 5′-CAGGGCACTGTAGATGGTCT-3′
TRAP	F, 5′-CAGCAGCTCCCTAGAAGATGG-3′ R, 5′-CACGGTTCTGGCGATCTCTT-3′
CTSK	F, 5′-TAGCACCCTTAGTCTTCCGC-3′ R, 5′-CTTGAACACCCACATCCTGC-3′
MMP-9	F, 5′-GCCGACTTTTGTGGTCTTCC-3′ R, 5′-GGTACAAGTATGCCTCTGCCA-3′
TNF-α	F, 5′-TTCCCAAATGGCCTCCCT-3′ R, 5′-TGGGCTACAGGCTTGTCACTC-3′
IL-6	F, 5′-CTTGGGACTGATGCTGG-3′ R, 5′-GGTCTGTTGGGAGTGGTAT-3′
IL-10	F, 5′-GGGTTGCCAAGCCTTATCG-3′ R, 5′-TCACTCTTCACCTGCTCCACT-3′

Animals and surgical procedure, dynamic histomorphometry

Fifty 8-week-old C57BL/J6 male mice were utilized to establish the model of particle-induced osteolysis in calvaria. All experiments involving animals were approved by the Institutional Review Board of Xijing Hospital (Permit No. 20161003). All methods were performed in accordance with National Institute of Health Guide for the Care and Use of Laboratory Animals. Mice were divided into 3 groups randomly (sham, control, metformin, $n = 15$/group, 5 for Micro-CT and dynamic histomorphometry, 5 for HE staining, TRAP staining, ALP staining, immunohistochemical staining, and immunofluorescence, 5 for RT-PCR, and ELISA). Surgical implantation of UHMWPE particles was performed as described in a previous report [10]. For surgery, mice were placed under general anesthesia via inhalation of isoflurane. An area (0.5×0.5 cm^2) of the periosteum was exposed via a midline sagittal incision of 10 mm on the calvaria. In both groups, a sterile sharp surgical spoon was used to uniformly distribute 20 µg of particles over the intact periosteum. A simple, interrupted 4-0 Ethicon suture was utilized to close the incision. The mice were subsequently placed into cages and provided food and water ad libitum. All animals were given metformin or normal saline

as control via local injection every day after surgery. Mice for dynamic histomorphometry were given two fluorescent bone formation markers calcein on day 3 and tetracycline 10 days after surgery through intraperitoneal injection. The animals were sacrificed 14 days after the operation via an overdose of intraperitoneal sodium pentobarbital. Soft tissue was dissected from the bones, and the elliptical plate of bone was removed carefully, to obtain the calvaria. After fixation with 90% ethanol, calvaria were cut at 1 mm thickness. All sections were captured with Olympus Inverted Fluorescence Microscope. Images were analyzed and mineral apposition rate (MAR) was defined according to the ASBMR standard guideline.

Micro-CT analysis

Dissected samples fixed in paraformaldehyde were utilized for in vitro examination of the calvarial bone structure via high-resolution micro-CT (eXplore Locus SP; GE Healthcare, Madison, WI, USA). The voltage, current, and integration time were 80 kV, 80 mA, and 3000 ms, with 14 mm resolution, respectively. A region of interest (ROI) was selected as the largest osteolytic volume that fit in a $152 \times 152 \times 152$ voxel template (85.2 mm^3). The data analysis was performed using commercial software (MicroView ABA ver. 2.1.2, GE Healthcare). Three parameters, i.e., bone mineral content (BMC), bone mineral density (BMD), and the ratio of bone volume to tissue volume (BV/TV), were used to evaluate the particle-induced osteolysis.

H&E, Masson staining, ALP staining, TRAP staining, and Alizarin Red S staining

Harvested mouse calvaria samples were decalcified in 10% EDTA solution for histologic evaluation. An acid phosphatase kit from Sigma-Aldrich and tartrate-resistant acid phosphatase (TRAP) stain were used to quantify osteoclasts, and the sagittal suture area was observed via hematoxylin and eosin (H&E) staining. The degree of osteolysis was evaluated in three neighboring sections under a microscope (Olympus BX 51, Tokyo, Japan). A computer running the OsteoMeasure Analysis system (OsteoMetrics, Decatur, GA, USA) was attached. Each image was oriented with a midline suture of 1.3 mm in diameter in the field center and was captured at magnitude 40×. Soft tissues and the area of osteolysis were traced manually under 40× magnification in H&E stain slices, and quantified with the image analysis system mentioned above. Alkaline phosphatase staining was performed with BCIP/NBT Alkaline Phosphatase Colour Development Kit (Beyotime, Jiangsu, China) according to the manufacturer's instructions. Mature osteocyte with BCP particles were cultured on coverslips, fixed with paraformaldehyde, and confirmed using H&E, ALP, and Masson staining. ALP-quantified activity was measured using Alkaline Phosphatase Assay Kit (Beyotime, Jiangsu, China) according to the manufacturer's instructions. Alizarin Red S staining was performed using 10% alizarin red (Sigma-Aldrich, USA) after fixation with paraformaldehyde.

Immunohistochemical staining and Immunofluorescence

The calvaria samples of mice were collected and fixed in paraformaldehyde. Samples were dehydrated, embedded in paraffin before sectioned at a thickness of 5 μm, and were used for each of the following staining. Sections were deparaffinized, treated with citric acid solution for the antigen retrieval, and then incubated with anti-SOST, DKK1, OPG, and RANKL antibody or p-AMPK antibody (diluted in 1:250). IHC staining was performed using the VECTASTAIN Elite ABC Kit (Vector Laboratories Inc.). Sections were then counterstained with hematoxylin, dehydrated through alcohol gradient, and examined under the light microscope. For fluorescence, detection of calvaria sections in three groups was prepared as previously described in immunohistochemical staining. Briefly, sections were incubated with antibody to CD11b (Cell Signaling, Danvers, MA, USA) and Ly6G (Phoenix Pharmaceuticals, Burlingame, CA, USA), and further incubated with fluorescent-labeled secondary antibodies. Stained sections were photographed digitally using an inverted fluorescence microscope (Nikon TE2000, Japan). The image was observed and collected (Ultraviolet excitation wavelength 330–380 nm, transmitting wavelength of 420 nm; FITC green light excitation wavelength 465–495 nm, transmitting wavelength of 515–555 nm; CY3 red light excitation wavelength is 510–560, transmitting wave length of 590 nm).

Western blot

In osteocytes, the cytoplasmic and nuclear lysates were obtained by lying directly with RIPA (Thermo Fisher Scientific) according to the manufacturer's instructions. Concentrations of proteins were determined using the BCA Protein Assay Kit (Thermo Fisher Scientific, USA). Protein extraction and immunoblot analysis were performed as previously described. Primary antibodies used in this study were phosphor-AMPKα(Thr172) (Cell Signaling Technology, USA). Secondary antibodies used in this study were rabbit immunoglobulin G-horseradish peroxidase (Solarbio, Beijing, China). Signals were detected using the Bio-Rad system (Bio-Rad, Hercules, CA, USA), and the densitometric analysis was performed using the Quantity One software (Bio-Rad, Hercules, CA, USA). Expression of GAPDH was used as the internal standard.

Statistical analysis

All data in vitro and in vivo were expressed as mean ± SD and analyzed for statistical significance using the one-way ANOVA. Every single experiment was repeated at least three times, and representative results are shown. For the study, $P < 0.05$ was considered significant.

Results

Metformin protects bone and reduces inflammation in UHWMPE particle-induced osteolysis mouse model

Mouse calvaria harvested 14 days after surgical implantation of UHMWPE particles were qualitatively and quantitatively analyzed by micro-CT (Fig. 1a). The low-signal area represents the sagittal suture area with neighboring bone resorption. The area of bone resorption observed following implantation of the UHMWPE particles was reduced by metformin treatment compared with that in mice received no further treatment. From 3D reconstruction imaging, bone quantity and quality were evaluated according to the BMD and BMC of ROIs (Fig. 1b). Both parameters were the lowest in the mice calvaria implanted with UHMWPE particles and given no further treatment, and the bone resorption reaction was evident. With daily metformin treatment, BMD and BMC of the calvaria were higher than those without additional treatment following particle implantation. HE staining shows less bone erosion in metformin-treated groups compared with control group. TRAP staining shows more positive cells in control group, quantified results show marked difference between control and metformin-treated group (Fig. 1c, d). Immunofluorescence shows less CD11b- and Ly6G-positive cells in metformin-treated group (Fig. 1f). Together with changes in inflammation markers TNF-α, IL-6, and anti-inflammation marker IL-10 (Fig. 1e), there is less inflammation after metformin administration.

Metformin reduces SOST and DKK1, and increases OPG in UHWMPE particle-induced osteolysis mouse model

To study the mechanisms of the inhibitory effect of metformin on particle-induced osteolysis, dominant regulators in bone metabolism were examined. RT-PCR results showed that particle implantation stimulated SOST, DKK1, and RANKL mRNA expression, and suppressed OPG mRNA expression in calvaria. However, metformin treatment inhibited these effects on cytokine production (Fig. 2a). Analysis of the cytokine production in organ culture suggested that SOST, DKK1, and RANKL production greatly increased upon exposure to particles and metformin treatment again significantly suppressed the particle's effect on negative regulators of bone formation. In addition, metformin treatment increased release of OPG. Consistent with the results of qRT-PCR, the results of ELISA also suggested that metformin had a potent effect on mature osteocyte (Fig. 2b). IHC staining shows similar results compared with the control group (Fig. 2c). As can be seen in Fig. 2d, the number of osteoblasts in metformin group increased compared with control group (indicated by quantified results). Calcein and tetracycline double fluorescent markers showed that the mineral deposition rate (MAR, μm/day) was higher in the metformin group than in the control group (Fig. 2e).

Metformin enhance osteoblasts proliferation and differentiation while inhibits osteoclastogenesis in 3D culture system

To investigate the effects of metformin on osteoblasts and osteoclastogenesis through mature osteocyte system, we use 3D culture system as previously described by Boukhechba [14]. Mature osteocytes were planked in each well and confirmed with staining (Fig. 3a, b) and RT-PCR (Fig. 3c) after differentiation. Osteoblasts or primary bone marrow macrophages (BMMs) were added to each insert for checking influence on osteoblast maturation and osteoclastogenesis. Treatment of osteocytes in wells but not inserts with metformin (10–50 μM) for 24 h led to a dose-dependent increase of osteoblast proliferation as determined by CCK-8 assay. Metformin affected alkaline phosphatase activity in osteoblasts in a dose-dependent manner (Fig. 3d). Furthermore, the effects of the anti-diabetic drug on osteoclastogenesis were also detected. After treating mature osteocyte with metformin for 3 days, TRAP staining showed less TRAP-positive cells in transwell insert in metformin-treated group. The effect is dose-dependent (Fig. 3e, f). Our results indicate that metformin acts as an osteogenic role in mature osteocyte system by enhancing osteoblast proliferation and inhibiting osteoclastogenesis.

Metformin reduce SOST and DKK1 secretion by osteocytes, and increase OPG/RANKL ratio

To further detect the mechanism of metformin affecting osteoblast and osteoclastogenesis in mature osteocyte system, we detected the level of main cytokines secreted by osteocytes. RT-PCR showed decreased level of SOST, DKK1, RANKL, and elevated level of OPG mRNA expression in metformin group as compared with control group with UHMWPE particles (Fig. 4a–d). SOST, DKK1, RANKL, and OPG levels were measured in the conditioned medium by ELISA assay. Negative regulator, SOST, DKK1, and RANKL were lower in

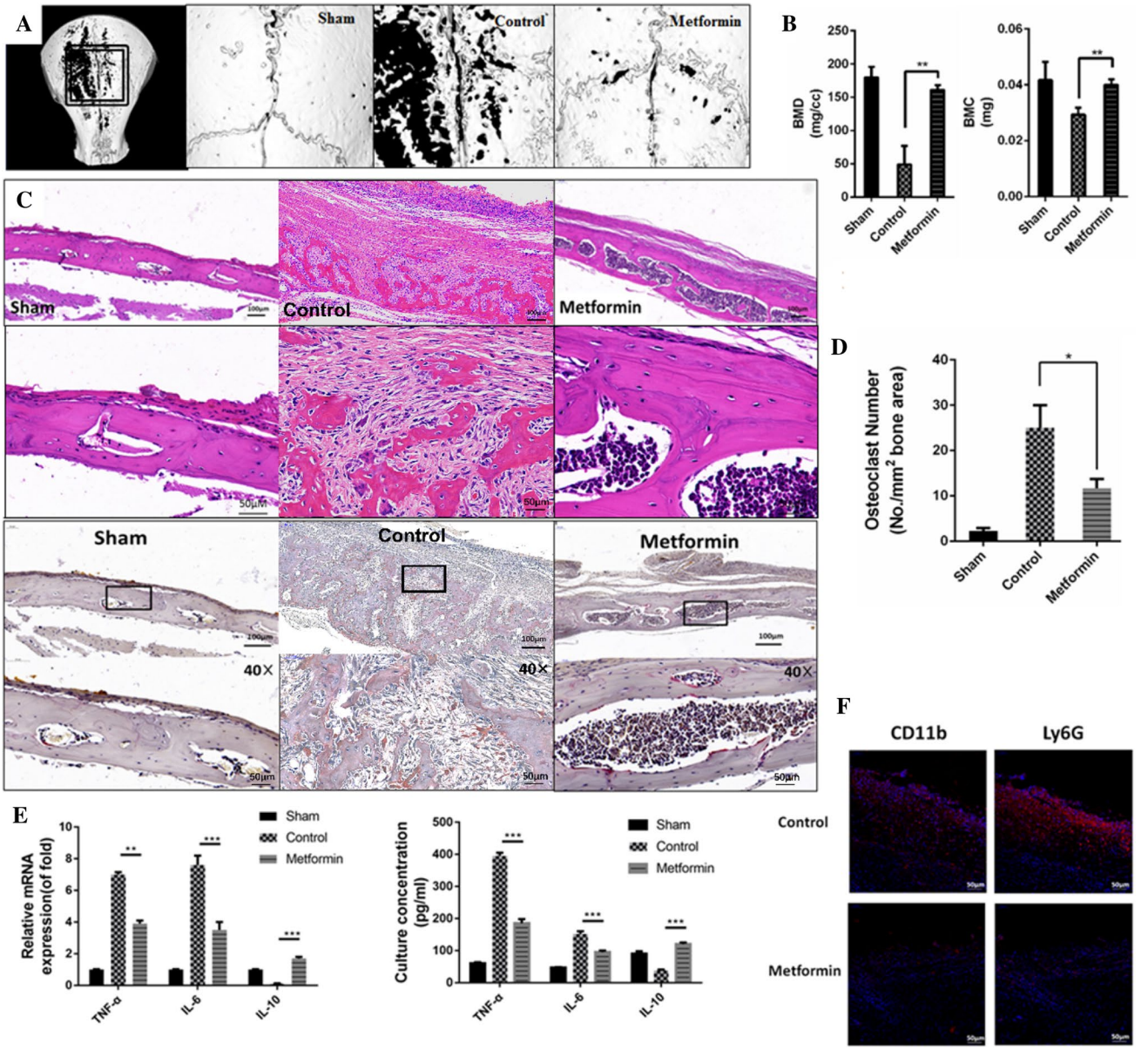

Fig. 1 Metformin protects bone and reduces inflammation in UHWMPE particle-induced osteolysis mouse model. Micro-CT results of mouse osteolysis model (**a**) shows increased erosion area in control group and reduced bone resorption in metformin group in accordance with quantified results (**b**) of BMD and BMC. HE staining shows decreased inflammation after metformin treatment (**c**). TRAP staining of bone tissue suggests more positive cells in control group and less positive ones after metformin treatment (**d**). Treatment with metformin significantly reduces the increase in expression of both TNF-α and IL-6, but enhances the release of IL-10 after exposure to the particles (**e**). Immunofluorescence staining shows less CD11b- and Ly6G-positive markers in metformin-treated group. Black rectangle indicates region of interest. *BMD* bone mineral density, *BMC* bone mineral content, *HE staining* hematoxylin–eosin staining, *TRAP staining* tartrate-resistant acid phosphatase staining. Data were collected from two sections per mouse and three mice per group. Data are presented as mean number ± SD (*$p < 0.05$; **$p < 0.01$; ***$p < 0.001$, $n = 3$). Representative data of at least three independent experiments are shown

metformin-treated group (of control group). OPG, a decoy receptor for RANKL, was higher in metformin-treated group (Fig. 4e–h). Compared with control group, the bone-protective OPG/RANKL ratio increased in metformin group according to Fig. 4i, j. Considering the functions of these regulators on bone metabolism, these changes indicated that metformin affects both osteoblast and osteoclast in an endocrinic way.

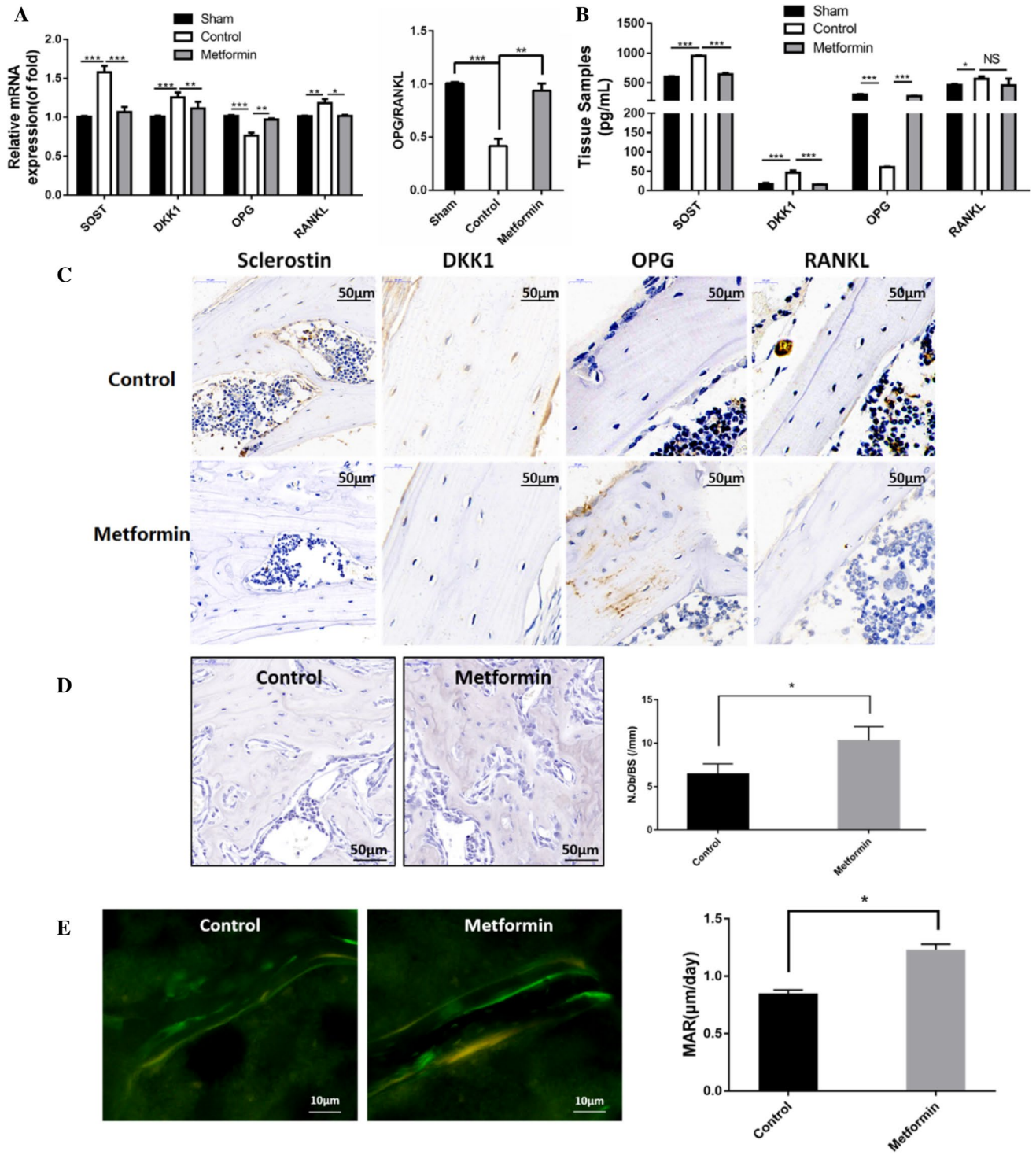

Fig. 2 Metformin changes regulator expression in mouse calvaria osteolysis model. Both RT-PCR (**a**) and ELISA (**b**) indicate SOST and DKK1 increase, while OPG/RANKL reduces in control group. Metformin reverses the effects, as is shown in immunohistochemical staining (**c**). **d** ALP staining shows that the number of osteoblasts in metformin group increases compared with control group (indicated by quantified results). Calcein and tetracycline double fluorescent markers show that the mineral deposition rate (MAR, μm/day) is higher in the metformin group than in the control group (**e**). *RT-PCR* real-time PCR, *ELISA* enzyme-linked immuno sorbent assay, *DKK1* Dickkopf-1, *OPG* osteoprotegerin, *RANKL* Receptor Activator of Nf-κB Ligand. Data are presented as mean number ± SD (*$p < 0.05$; **$p < 0.01$; ***$p < 0.001$, $n = 3$). Data were collected from at least three mice per group. Representative data of at least three independent experiments are shown

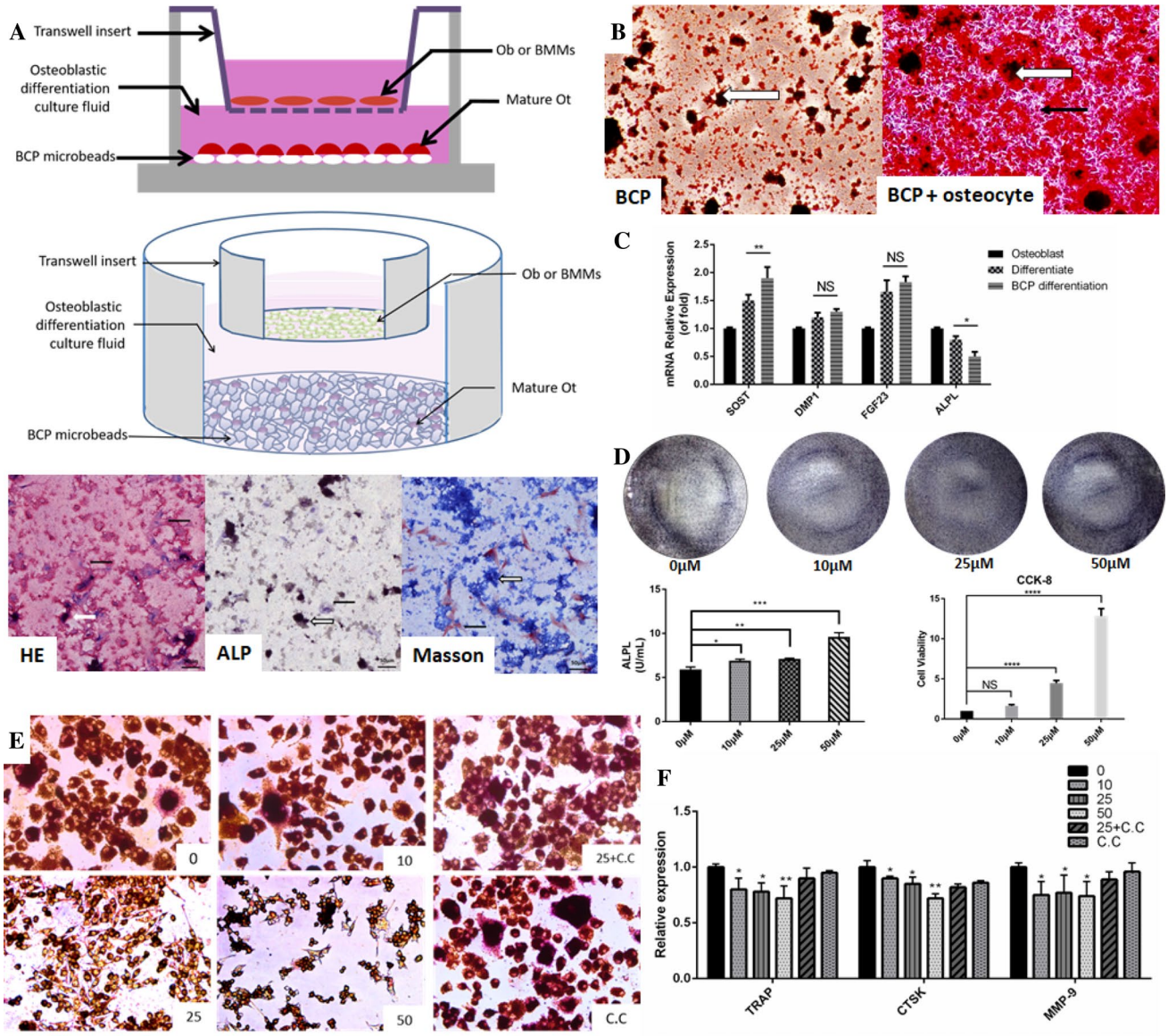

Fig. 3 Metformin enhances osteoblasts proliferation and differentiation while inhibits osteoclastogenesis in 3D culture system. Construction of 3D mature osteocyte system with transwell (**a**). White arrows indicate BCP particles and black arrows indicate osteocytes. **b** Mature osteocytes are confirmed with Alizarin Red S staining. RT-PCR (**c**) after 3 weeks of differentiation shows that osteocyte in 3D system is more differentiated than those differentiated without BCP particles. ALP staining and CCK-8 suggest increased ALP activity and cell viability in metformin-treated group (**d**). TRAP staining (**e**) and RT-PCR (**f**) results indicate a dose-dependent decrease in osteoclastogenesis. Compound C blocked these effects on osteoclasts. *Ob* osteoblast, *BMMs* bone marrow-derived macrophages, *Ot* osteocyte, *BCP* biphasic calcium phosphate, *SOST* sclerostin, *DMP1* dentin matrix protein 1, *FGF23* fibroblast growth factors 23, *ALPL* alkaline phosphatase, *C.C* Compound C, *TRAP* tartrate-resistant acid phosphatase, *CTSK* cathepsin K, *MMP-9* metalloproteinase-9. Data are presented as mean number ± SD (*$p < 0.05$; **$p < 0.01$; ***$p < 0.001$, $n = 5$ technical replicates). Representative data of at least three independent experiments are shown

Blocking AMPK phosphorylation reverses secretion of OPG induced by metformin

To identify whether the changes in bone regulators were connected with metformin's action as an AMPK activator, we added AMPK signal pathway inhibitor, compound C, together with metformin into mature osteocyte system. Western blot shows that AMPK phosphorylation is blocked after Compound C treatment (Fig. 4k). Both RT-PCR and ELISA show no difference in SOST, DKK1, and RANKL secretion in both groups (data not shown). However, there is a considerable difference in OPG secretion between both groups (Fig. 4c, g), indicating that elevated OPG might be an effect of AMPK signal pathway activation. The ELISA result

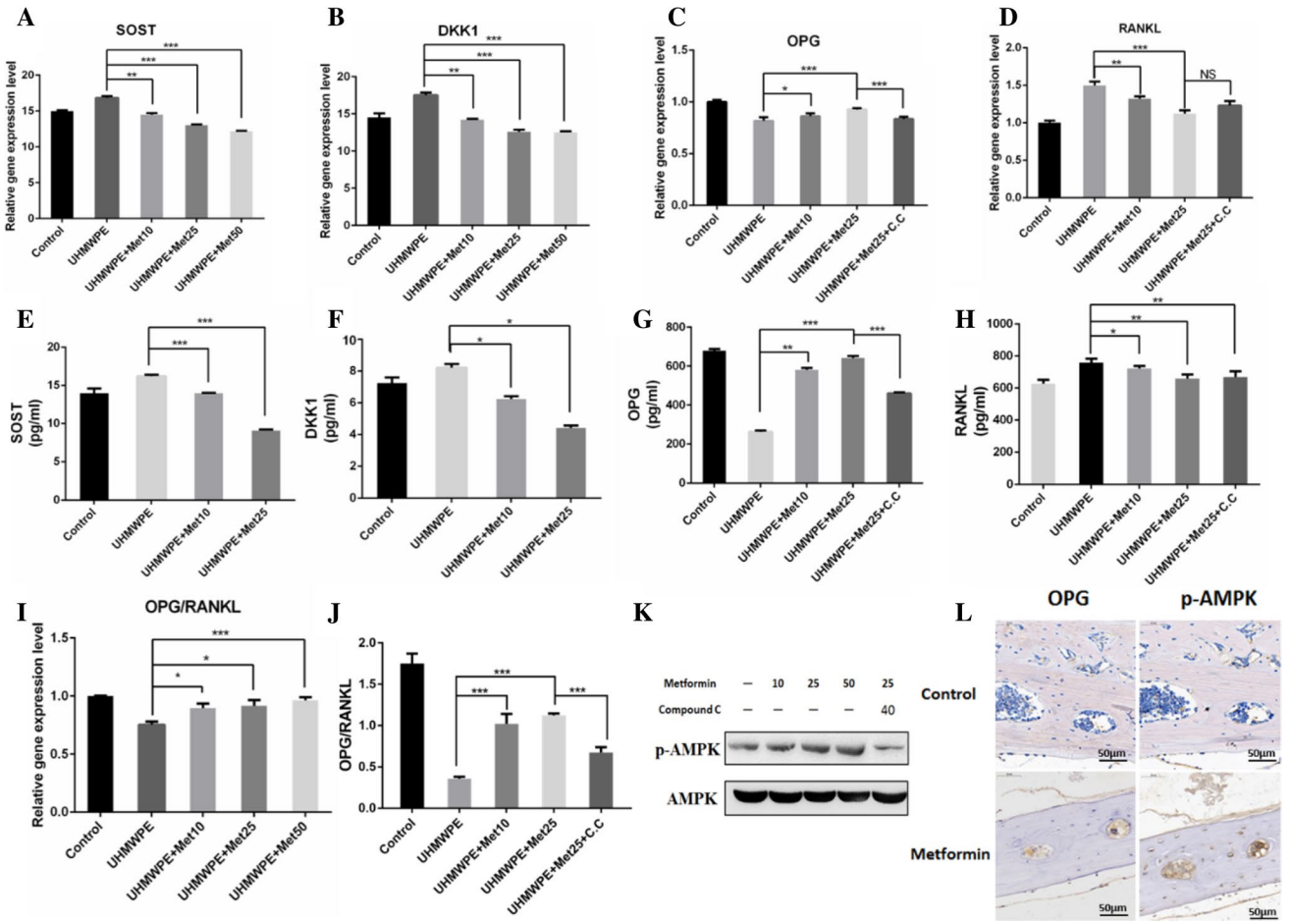

Fig. 4 Metformin reduces SOST and DKK1 secretion by osteocytes, and increases OPG/RANKL ratio. RT-PCR and ELISA results show a dose-dependent decrease of SOST (**a**, **d**) and DKK1 (**b**, **e**), and increased OPG/RANKL ratio (**c**). Treatment with compound C decreases OPG (**f**) and p-AMPK (**g**) levels at a large scale. Immunohistochemical staining of OPG and p-AMPK at adjacent sections shows increased positive cells in metformin-treated group (**h**). *Met* metformin, *C.C* compound C. Data are presented as mean number ± SD (*$p < 0.05$; **$p < 0.01$; ***$p < 0.001$, $n = 5$ technical replicates). Representative data of at least three independent experiments are shown

coincides with TRAP staining and RT-PCR of osteoclast markers (Fig. 3e, f), suggesting a close connection between metformin's AMPK activation role and the osteoclastogenesis inhibition effect. IHC staining of adjacent sections shows more OPG and p-AMPK-positive cells in metformin-treated group (Fig. 4h).

Discussion

Over 90% of the bone cells in the adult skeleton are osteocytes, and the ratio is increasing with age and size of the bone [15, 16]. It has been long acknowledged that bone is anything but an endocrine gland. Recent discoveries have shown that mature osteocytes in mineralized bone matrix, indeed, play multifunctional role in bone homeostasis via many key regulators [17]. Osteocytes change the state of osteoblasts and osteoclasts in response to stimulations by producing factors (SOST, DKK1, RANKL, and OPG) that affect other bone cells in a paracrine or autocrine way, and secrete hormones (FGF23) that influence other tissues in an endocrine way [18–21].

Sclerostin and DKK1 are two inhibitors of canonical Wnt signaling pathways most secreted by osteocytes, which regulate transcription of genes that promote osteoblastic bone formation by binding to LRP5 and 6 to prevent formation of the Frizzled/LRP receptor complex and thus Wnt-mediated signaling [22, 23]. Osteocytes also produce cytokines that regulate osteoclastogenesis involving activation of the receptor activator of nuclear factor κB (RANK) by RANKL, which is mainly produced by osteocytes [24]. OPG, competitive inhibitor of RANKL, which strongly inhibit osteoclast differentiation, is also a product of osteocytes [25, 26]. Using genetically modified mice with deletion of RANKL

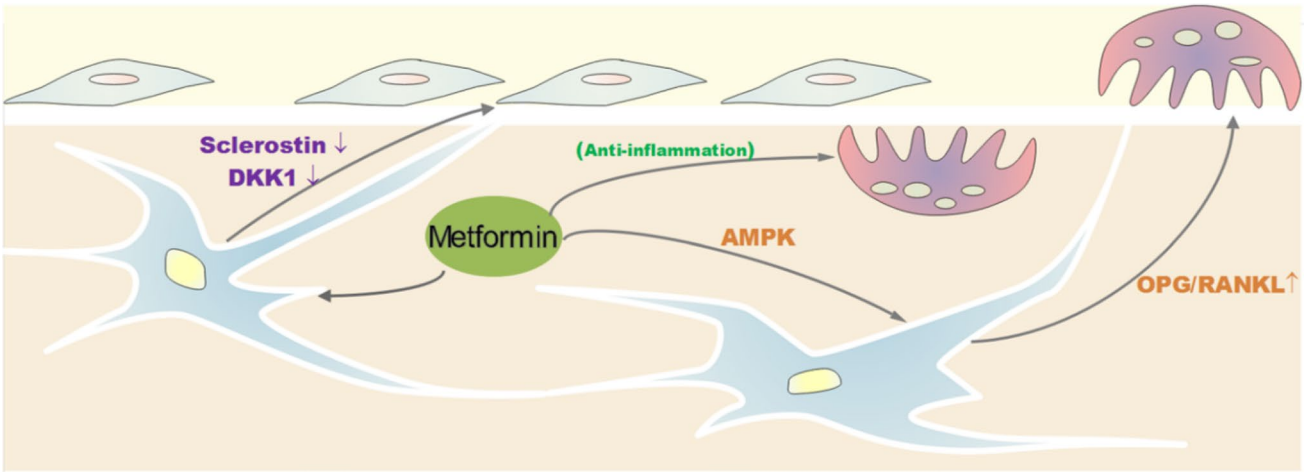

Fig. 5 Metformin reduces inflammation, inhibits SOST and DKK1, and increases OPG/RANKL ratio in UHMWPE particle-induced osteolysis

from osteocytes, researchers suggest that osteocytes are the main source of RANKL [27].

Dysregulated bone formation and/or bone resorption may lead to bone metabolic disorder, such as osteoporosis, multiple myeloma, and osteolysis, which is recently found to be connected with abnormal bone regulators, as well [28–31]. UHMWPE particles induce aseptic inflammation and further promote osteoclastogenesis and bone resorption. Meanwhile, osteoblasts proliferation is inhibited by particle stimulation [32]. As new therapeutics need to be found and stress regulation remains far from application, endocrinic function of osteocyte should be considered in new strategies to prevent and treat bone disease. Metformin's bone-protective property in diabetic patients is generally accepted. However, its effect on bone metabolism has not been fully explored, especially in some bone disorders. Researchers found that metformin had an effect on circulating bone markers like SOST [33–35]. This may be translated into a bone formation-promoting effect. In other studies, metformin played an anti-inflammation role in cardiovascular diseases [36, 37].

We used the recognized calvarial model with direct exposure to UHMWPE particles to simulate aseptic osteolysis in vivo and detected the effect of metformin on this process. The anti-inflammation effects were explored in our previous work. Here, we mainly explored its bone-protective effect. There was a marked increase in the number of osteoclasts and bone erosion in the calvaria of mice exposed to wear particles. Metformin reduced bone loss, abated inflammation, and lowered the number of osteoclasts present in a dose-dependent manner. In addition, metformin treatment led to a decrease in SOST and DKK1 secretion as well as an increase the bone protecting OPG/RANKL ratio. We then explored the effects in vitro. Since current osteocyte models had some disadvantages, we used the latest 3D mature osteocyte culture system performed by Boukhechba [14]. Metformin inhibited the secretion of SOST and DKK1 by osteocytes, and elevated OPG/RANKL ratio in a dose-dependent manner. Moreover, experiments with AMPK inhibitor Compound C show that the effects of metformin on OPG are dependent on AMPK activation, proving that the regulation of OPG may be related to the activation of a serine/threonine protein kinase of AMPK, which is critical in maintaining metabolic homeostasis in eukaryotic cell types [38]. Therefore, we hypothesized that metformin reduced inflammation, which led to inhibited osteoclastogenesis and bone resorption. Moreover, SOST and DKK1, inhibitors of canonical Wnt signaling pathways most secreted by osteocytes were reduced upon metformin administration and OPG/RANKL ratio increased (Fig. 5). Taken together, the anti-diabetic drug had a bone-protective property in UHMWPE particle-induced osteolysis.

In summary, the present study provides evidence that metformin influences bone metabolism in an endocrine way, therefore, providing the possibility that it might be used clinically to treat peri-implant aseptic loosening. Given that osteocytes account for a great proportion in bone tissue and recently have been found to play an endocrine role in bone metabolism, the regulation of osteocyte secretion may be much more effective than the previous treatment. Moreover, since metformin functions by decreasing glucose production in the liver and intensifying the sensitivity of insulin, particularly in people who are overweight and often found in patients with osteoporosis and TJA patients, metformin may represent a promising therapeutic agent for preventing or correcting periprosthetic osteolysis and other bone diseases [39–41].

Acknowledgements This work was supported by the Project of Natural Science Foundation of Shaanxi Province (2014JQ4142) and

the National Natural Science Foundation of China (81501936) and (31571215).

Compliance with ethical standards

Conflict of interest None of the authors have conflict of interest.

References

1. Inacio MC, Ake CF, Paxton EW, Khatod M, Wang C, Gross TP, Kaczmarek RG, Marinac-Dabic D, Sedrakyan A (2013) Sex and risk of hip implant failure: assessing total hip arthroplasty outcomes in the United States. JAMA Intern Med 173:435–441
2. Sellmeyer DE (2010) Atypical fractures as a potential complication of long-term bisphosphonate therapy. JAMA 304:1480–1484
3. Lee NK, Sowa H, Hinoi E, Ferron M, Ahn JD, Confavreux C, Dacquin R, Mee PJ, McKee MD, Jung DY, Zhang Z, Kim JK, Mauvais-Jarvis F, Ducy P, Karsenty G (2007) Endocrine regulation of energy metabolism by the skeleton. Cell 130:456–469
4. Liu S, Zhou J, Tang W, Jiang X, Rowe DW, Quarles LD (2006) Pathogenic role of Fgf23 in Hyp mice. Am J Physiol Endocrinol Metab 291:E38–E49
5. Hegazy SK (2015) Evaluation of the anti-osteoporotic effects of metformin and sitagliptin in postmenopausal diabetic women. J Bone Miner Metab 33:207–212
6. Jeyabalan J, Viollet B, Smitham P, Ellis SA, Zaman G, Bardin C, Goodship A, Roux JP, Pierre M, Chenu C (2013) The anti-diabetic drug metformin does not affect bone mass in vivo or fracture healing. Osteoporos Int 24:2659–2670
7. Jang WG, Kim EJ, Bae IH, Lee KN, Kim YD, Kim DK, Kim SH, Lee CH, Franceschi RT, Choi HS, Koh JT (2011) Metformin induces osteoblast differentiation via orphan nuclear receptor SHP-mediated transactivation of Runx2. Bone 48:885–893
8. Araújo AA, Pereira ASBF, Medeiros CACX, Brito GAC, Leitão RFC, Araújo LS, Guedes PMM, Hiyari S, Pirih FQ, Araújo Júnior RF (2017) Effects of metformin on inflammation, oxidative stress, and bone loss in a rat model of periodontitis. PLoS One 12:e0183506
9. Wang P, Ma T, Guo D, Hu K, Shu Y, Xu HHK, Schneider A (2018) Metformin induces osteoblastic differentiation of human induced pluripotent stem cell-derived mesenchymal stem cells. J Tissue Eng Regen Med 12:437–446
10. Jablonski H, Polan C, Wedemeyer C, Hilken G, Schlepper R, Bachmann HS, Grabellus F, Dudda M, Jäger M, Kauther MD (2017) A single intraperitoneal injection of bovine fetuin-A attenuates bone resorption in a murine calvarial model of particle-induced osteolysis. Bone 105:262–268
11. Sun Q, Gu Y, Zhang W, Dziopa L, Zilberberg J, Lee W (2015) Ex vivo 3D osteocyte network construction with primary murine bone cells. Bone Res 3:15026
12. Shah M, Kola B, Bataveljic A, Arnett TR, Viollet B, Saxon L, Korbonits M, Chenu C (2010) AMP-activated protein kinase (AMPK) activation regulates in vitro bone formation and bone mass. Bone 47:309–319
13. Takahashi N, Akatsu T, Udagawa N, Sasaki T, Yamaguchi A, Moseley JM, Martin TJ, Suda T (1988) Osteoblastic cells are involved in osteoclast formation. Endocrinology 123:2600–2602
14. Boukhechba F, Balaguer T, Michiels JF, Ackermann K, Quincey D, Bouler JM, Pyerin W, Carle GF, Rochet N (2009) Human primary osteocyte differentiation in a 3D culture system. J Bone Miner Res 24:1927–1935
15. Bonewald LF (2007) Osteocytes as dynamic multifunctional cells. Ann N Y Acad Sci 1116:281–290
16. Manolagas SC, Parfitt AM (2013) For whom the bell tolls: distress signals from long-lived osteocytes and the pathogenesis of metabolic bone diseases. Bone 54:272–278
17. Dallas SL, Prideaux M, Bonewald LF (2013) The osteocyte: an endocrine cell… and more. Endocr Rev 34:658–690
18. Henriksen K, Neutzsky-Wulff AV, Bonewald LF, Karsdal MA (2009) Local communication on and within bone controls bone remodeling. Bone 44:1026–1033
19. Henriksen K, Karsdal MA, Martin TJ (2014) Osteoclast-derived coupling factors in bone remodeling. Calcif Tissue Int 94:88–97
20. Koide M, Kobayashi Y, Yamashita T, Uehara S, Nakamura M, Hiraoka BY, Ozaki Y, Iimura T, Yasuda H, Takahashi N, Udagawa N (2017) Bone formation is coupled to resorption via suppression of sclerostin expression by osteoclasts. J Bone Miner Res 32:2074–2086
21. Martin T, Gooi JH, Sims NA (2009) Molecular mechanisms in coupling of bone formation to resorption. Crit Rev Eukaryot Gene Expr 19:73–88
22. Wang N, Xue P, Wu X, Ma J, Wang Y, Li Y (2018) Role of sclerostin and dkk1 in bone remodeling in type 2 diabetic patients. Endocr Res 43:29–38
23. Ke HZ, Richards WG, Li X, Ominsky MS (2012) Sclerostin and Dickkopf-1 as therapeutic targets in bone diseases. Endocr Rev 33:747–783
24. Xiong J, Piemontese M, Onal M, Campbell J, Goellner JJ, Dusevich V, Bonewald L, Manolagas SC, O'Brien CA (2015) Osteocytes, not osteoblasts or lining cells, are the main source of the RANKL required for osteoclast formation in remodeling bone. PLoS One 9:e0138189
25. Li CW, Liang B, Shi XL, Wang H (2015) Opg/Rankl mRNA dynamic expression in the bone tissue of ovariectomized rats with osteoporosis. Genet Mol Res 14:9215–9224
26. Wang L, Dai Z, Xie J, Liao H, Lv C, Hu Y (2016) Alteration of the RANKL/RANK/OPG system in periprosthetic osteolysis with septic loosening. Inflammation 39:218–227
27. Xiong J, Piemontese M, Thostenson JD, Weinstein RS, Manolagas SC, O'Brien CA (2014) Osteocyte-derived RANKL is a critical mediator of the increased bone resorption caused by dietary calcium deficiency. Bone 66:146–154
28. Almeida M, Han L, Martin-Millan M, Plotkin LI, Stewart SA, Roberson PK, Kousteni S, O'Brien CA, Bellido T, Parfitt AM, Weinstein RS, Jilka RL, Manolagas SC (2007) Skeletal involution by age-associated oxidative stress and its acceleration by loss of sex steroids. J Biol Chem 282:27285–27297
29. Weinstein RS, Wan C, Liu Q, Wang Y, Almeida M, O'Brien CA, Thostenson J, Roberson PK, Boskey AL, Clemens TL, Manolagas SC (2010) Endogenous glucocorticoids decrease skeletal angiogenesis, vascularity, hydration, and strength in aged mice. Aging Cell 9:147–161
30. Nicks KM, Amin S, Atkinson EJ, Riggs BL, Melton LJ 3rd, Khosla S (2012) Relationship of age to bone microstructure independent of areal bone mineral density. J Bone Miner Res 27:637–644
31. Ollivere B, Wimhurst JA, Clark IM, Donell ST (2012) Current concepts in osteolysis. J Bone Joint Surg Br 94:10–15
32. Howie DW, Neale SD, Haynes DR, Holubowycz OT, McGee MA, Solomon LB, Callary SA, Atkins GJ, Findlay DM (2013) Periprosthetic osteolysis after total hip replacement: molecular pathology and clinical management. Inflammopharmacology 21:389–396
33. van Lierop AH, Hamdy NA, van der Meer RW, Jonker JT, Lamb HJ, Rijzewijk LJ, Diamant M, Romijn JA, Smit JW, Papapoulos SE (2012) Distinct effects of pioglitazone and metformin on circulating sclerostin and biochemical markers of bone turnover in men with type 2 diabetes mellitus. Eur J Endocrinol 166:711–716

34. Kim MH, Jee JH, Park S, Lee MS, Kim KW, Lee MK (2014) Metformin enhances glucagon-like peptide 1 via cooperation between insulin and Wnt signaling. J Endocrinol 220:117–128
35. Sofer E, Shargorodsky M (2016) Effect of metformin treatment on circulating osteoprotegerin in patients with nonalcoholic fatty liver disease. Hepatol Int 10:169–174
36. Saisho Y (2015) Metformin and inflammation: its potential beyond glucose-lowering effect. Endocr Metab Immune Disord Drug Targets 15:196–205
37. Cao X, Li H, Tao H, Wu N, Yu L, Zhang D, Lu X, Zhu J, Lu Z, Zhu Q (2013) Metformin inhibits vascular calcification in female rat aortic smooth muscle cells via the AMPK-eNOS-NO pathway. Endocrinology 154:3680–3689
38. Hardie DG, Ross FA, Hawley SA (2012) AMPK: a nutrient and energy sensor that maintains energy homeostasis. Nat Rev Mol Cell Biol 13:251–262
39. Pawlyk AC, Giacomini KM, McKeon C, Shuldiner AR, Florez JC (2014) Metformin pharmacogenomics: current status and future directions. Diabetes 63:2590–2599
40. Jones CA, Cox V, Jhangri GS, Suarez-Almazor ME (2012) Delineating the impact of obesity and its relationship on recovery after total joint arthroplasties. Osteoarthr Cartil 20:511–518
41. Lavernia CJ, Heiner AD, Villa JM, Alcerro JC, Rossi MD (2017) Preoperative glycemic control on total joint arthroplasty patient-perceived outcomes and hospital costs. J Arthroplast 32:6–10